Aberrant regulation of serine metabolite drives extracellular vesicle release and cancer progression

Tomofumi Yamamoto[1,2], Jun Nakayama[2], Fumihiko Urabe[2], Kagenori Ito[2], Masahiko Kuroda[4], Yutaka Hattori[3], Yusuke Yamamoto[2*], & Takahiro Ochiya[1*]

1. Department of Molecular and Cellular Medicine, Institute of Medical Science, Tokyo Medical University, Tokyo, Japan.
2. Laboratory of Integrative Oncology, National Cancer Center Research Institute, Tokyo, Japan.
3. Clinical Physiology and Therapeutics, Keio University Faculty of Pharmacy, Tokyo, Japan.
4. Department of Molecular Pathology, Tokyo Medical University, Tokyo, Japan.

*corresponding authors

Corresponding to:

Takahiro Ochiya, Ph.D.

Professor,

Department of Molecular and Cellular Medicine,

Institute of Medical Science, Tokyo Medical University

6-7-1, Nishishinjyuku, Shinjyuku-ku, Tokyo 160-0023, Japan

Phone: +81- 3-3342-6111, ext. 67136

Fax: +81-3-6302-0265

E-mail: tochiya@tokyo-med.ac.jp

Yusuke Yamamoto, Ph.D.

Unit leader,

Laboratory of Integrative Oncology,

National Cancer Center Research Institute, Tokyo

5-1-1, Tsukiji, Chuo-ku, Tokyo 104-0045, Japan

Phone: +81- 3-3452-2511, ext. 3664

Fax: +81-3-3543-9305

E-mail: yuyamamo@ncc.go.jp

Abstract

Cancer cells secrete extracellular vesicles (EVs) to regulate cells in the tumor microenvironment for their own benefit to grow and survive in the patient's body. Although emerging evidence has demonstrated the molecular mechanisms of EV release, regulating cancer-specific EV secretion remains challenging. In this study, we applied a microRNA (miRNA) library to reveal the universal mechanisms of EV secretion in cancer cells. Here, we identified miR-891b and its direct target gene, phospho-aminotransferase 1 (PSAT1), which promotes EV secretion through the serine synthesis pathway. Inhibition of PSAT1 affected EV secretion in multiple types of cancer, suggesting that the miR-891b/PSAT1 axis shares a common mechanism of cancer EV secretion. Interestingly, PSAT1 also controlled cancer metastasis via EV secretion. Our data provide insights into the PSAT1-controlled EV secretion mechanism and its potential as a therapeutic target in multi types of cancer.

Introduction

Exosomes are small EVs (small-Extracellular Vesicles: sEVs) with a diameter of approximately 50–150 nm (1-2). In general, cancer cells secrete a large number of exosomes comparing to normal cells (3) to modify the tumor microenvironment and support the growth of tumor cells (4-6). Therefore, inhibiting exosome secretion by cancer cells will have therapeutic benefits to be a less tumor-promoting environment (7).

EV secretion can be generally divided into two pathways: the ESCRT-dependent pathway and the ESCRT-independent pathway. Exosomes are formed by inward budding into early endosomes, which becomes multivesicular bodies (MVBs), and released into the extracellular environment through MVB fusing to cellualr membrane (8-10). Alix and TSG101 are proteins related to the ESCRT endosomal pathway, while the ESCRT-independent pathway includes nSMase2, which is involved in ceramide synthesis (3, 11-12). One of the reasons for increase of secretion is that oncogenic signaling, such as signaling through MYC and RAS, promotes EV release (13). Recently, we reported that miR-26a regulates EV secretion from PC-3M prostate cancer cells by targeting SHC4, PFDN4 and CHORDC1, resulting in tumor suppression (14). Furthermore, EV secretion was regulated via miR-1908/spermidine synthase (SRM) in 22Rv1 prostate cancer cells (15). Thus, cancer cells seem to utilize a different EV secretion machinery from non-cancerous cells. Several small molecules regulate EV secretion. P2RX7 inhibitor, which suppresses the disease-related EV secretion, leading to attenuating the disease phenotype (16). GW4869 inhibits cancer cell-derived EV secretion; however, it also affected EV secretion from normal cells (17). Additionally, the cargo of EVs is important for cancer progression (18-20).

Our previos study reported that we bypassed the complicated EV purification process and examined the effect of each miRNA on EV secretion in a high-throughput manner by

ExoScreen method (21). To further elucidate the universal molecular mechanisms of EV secretion, we performed a miRNA library screen of cell lines from colorectal and lung cancer. In the process of performing the miRNA library screen, we used an ExoScreen assay to systematically quantify the EV amount. From the miRNA-based screen, we identified miR-891b, which suppressed EV secretion in cancer cell lines. Additionally, its one of direct target gene, phospho-aminotransferase 1 (PSAT1), which positively regulated EV secretion via the serine de novo synthesis pathway. Present study showed PSAT1-controlled EV secretion in multiple types of cancer cells and the contribution of PSAT1 to bone metastasis in breast cancer via EV secretion.

Results

miR-891b suppresses EV secretion from colon and lung cancer cell lines

To identify novel molecular mechanisms of EV secretion, we performed a miRNA-based screen of the HCT116 colon cancer and A549 lung adenocarcinoma cell lines using a miRNA mimic library (1728 miRNAs in total). The amount of EV in the conditioned medium collected from miRNA-transfected cells was measured by the ExoScreen, which we previously developed as an ultrasensitive EV detection method (21). To exclude miRNAs that decrease EV number through cellular death, we assessed the cellular proliferation simultaneously **(Figure 1a)**. To confirm EV secretion, surface markers of EVs, i.e., CD9 and CD63, were verified by Western blot analysis, and the EV size and particle number were evaluated by nanoparticle tracking analysis (NTA) **(Figure 1b, c)**. Among genes regulating EV secretion, TSG101 was used for a positive control for EV secretion screening **(Figure 1d)**. From the library of 1728 miRNAs, we excluded miRNAs that affected cell proliferation (CCK-8 signal normalized to that in negative control cells= < 0.8 or > 1.2) **(Figure 1e)**. After selection, the inhibitory effects of the miRNAs (z-scores) on EV secretion were quantified in both cell lines **(Figure 1f)**. As shown in **Figure 1g**, the top 10 miRNAs with the highest z-scores were selected. Two miRNAs, miR-891b and miR-526a, were selected in both cell lines (marked in red). We validated the efficacy of the selected miRNAs **(Supplementary Figure 1a)**, and focused on miR-891b for further analysis as the most effective miRNA. miR-891 decreased secretion of both CD9-positive EVs and CD63-positive EVs to 40-60% based on Exoscreen assay of conditioned medium and isolated EVs by ultracentrifugation **(Supplementary Figure 1b)**. The decrease of EV secretion was further verified by NTA **(Supplementary Figure 1c)**. Additionally, high expression of miR-891b was significantly

correlated with prognosis in lung adenocarcinoma, although the correlation was not statistically significant in rectal cancer **(Supplementary Figure 1d)**.

PSAT1 is one of the target genes of miR-891b

To investigate the molecular mechanism of miR-891b in EV secretion, we identified genes which EV secretion was suppressed by miR-891b. We performed a mRNA microarray analysis using HCT116 and A549 cells transfected with either a miR-891b mimic or a control mimic. In the microarray results, 2,221 and 4,711 genes were downregulated in miR-891b mimic-transfected HCT116 and A549 cells, respectively (fold change < -1.5). We also prepared a gene list that was predicted to be miR-891b target genes according to the TargetScan database (2,618 genes). Comparing the gene lists from microarray and from the target prediction, we selected 82 genes overlapped among all 3 groups (**Figure 2a, Supplemental Table 1)**. Based on a literature search, we selected 45 genes from these 82 genes that are likely related to endosome organization and lipogenesis. Then, we examined whether silencing of these 45 genes suppressed EV secretion, consistent with miR-891b transfection (**Figure 2b**). Attenuating PSAT1 gene expression significantly decreased CD9-positive and CD63-positive EVs in both cell lines (**Figure 2c, d**). The particle number of EVs secreted from PSAT1-knockdown cells was also decreased significantly (**Figure 2e**). In addition to PSAT1, we identified other candidate genes, PDXK, RAB31, and VPS37B, that decreased EV secretion **(Supplementary 2a)**. Although the effect of VPS37B on EV secretion was not verified by NTA, silencing of PDXK and RAB31 decreased the particle number of EVs **(Supplementary 2b)**.

Next, we examined whether PSAT1 is a direct target of miR-891b. The PSAT1 mRNA expression and protein amount were significantly decreased after transfection with the miR-891b mimic, as confirmed by qRT–PCR (**Figure 2f**) and Western blotting (**Figure 2g**). Then, we

conducted a luciferase 3'UTR reporter assay to examine whether miR-891b can directly bind to the 3'UTR of PSAT1. We constructed assay vectors with several sequence variations, including the predicted miR-891b target sequences (**Figure 2h**). The assay revealed that wild-type PSAT1 3'UTR, but not other variants, was suppressed by miR-891b (**Figure 2i**). These results revealed that PSAT1 is directly targeted by miR-891b.

We next examined EV biogenesis after PSAT1 siRNA transfection. Immunofluorescence staining of CD63 as EV surface marker (green) and PSAT1 (red) showed accumulation of CD63 signals in the cytoplasm after PSAT1 silencing **(Figure 3a)**. Likewise, accumulation of CD63 signals was observed after miR-891b transfection **(Supplementary Figure 3a)**. This observation suggests that PSAT1 silencing led to EV retention in the cytoplasm but did not inhibit EV formation. To further elucidate the role of PSAT1 on EV biogenesis in detail, we co-immunostained CD63 with the early endosome marker EEA1 or the late endosome marker Rab7. As shown in **Supplementary Figure 3b**, very little overlap between EEA1 and CD63 was observed in either NC or siPSAT1, while the majority of CD63 and Rab7 overlapped following NC control. Introducing siRNA for PSAT1 caused less colocalization of CD63 and Rab7 (**Figure 3b, c; Supplementary Figure 3c**).

The serine synthesis pathway via PSAT1 contributes to EV secretion in cancer

Since PSAT1 is a famous regulator gene in serine synthesis pathway **(Figure 4a)**, we investigated the importance of serine synthesis in EV biogenesis. A serine-depleted medium was used for examination of the the impact of serine on EV secretion **(Figure 4b)**. As expected, while siPSAT1-transfected cells grew at a similar speed in a normal culture medium, siPSAT1-transfected cancer cells grew slower in the serine-depleted medium. We next investigated whether serine depletion influences EV secretion, and whether adding serine can rescue EV secretion in

siPSAT1-transfected cancer cells. As shown in EV quantification results by ExoScreen **(Figure 4c, d)** and NTA **(Figure 4e, f)**, serine depletion decreased EV secretion level to 30-40% in PSAT1 knock-down cells when normalized by cell number, and supplementing serine restored EV secretion to a similar level to control samples . These data indicated that PSAT1-mediated serine synthesis is responsible for EV secretion.

To further confirm the importance of the serine synthesis pathway for EV secretion, we performed knock-down experiments for PHGDH, which is upstream of PSAT1, and PSPH, which is downstream of PSAT1 in the serine synthesis pathway. The knock-down efficiency of PHGDH and PSPH by siRNAs was confirmed in the HCT116 and A549 cell lines at the protein level **(Figure 4g, h)**. As expected, PHGDH silencing significantly decreased EV secretion in both cell lines, while the EV number was significantly decreased only in A549 cells after PSPH silencing (**Figure 4i)**. Cell proliferation was not changed after knock-down, although PSPH siRNA slightly reduced the cell number in A549 cells (**Figure 4j**). These data further confirmed the serine synthesis pathway contributes to EV secretion in cancer cells.

PSAT1 regulates EV secretion in multiple cancer cell lines

We sought to examine whether the PSAT1-controlled EV secretion mechanism is shared in other cancer and normal cells. First, we evaluated the expression levels of PSAT1 in colorectal cancer cell lines (HCT15, COLO201, COLO205, and HT-29), normal colon fibroblasts (CCD-18co), lung cancer cell lines (A427, H1650, and H2228), and normal lung epithelial cells. The expression levels of PSAT1 were generally higher in both types of cancer cells than in the corresponding normal cell lines **(Figure 5a)**. Additionally, the PSAT1 expression level was positively correlated with EV secretion (**Figure 5b**). Then we analyzed the PSAT1 expression levels in clinical samples deposited in a public database Oncomine. We confirmed the higher expression of PSAT1

in colon, lung, ovarian, breast, melanoma, head-neck and multiple myeloma but not pancreas (**Figure 5c)**. Furthermore, a high expression level of PSAT1 was associated with overall survival in lung cancer patients, particularly at the early stage. **(Figure 5d)**. In colorectal cancer, previous study reported that a high expression level of PSAT1 was found to be related to poor prognosis (22). Additionally, a high expression level of PSAT1 was related to poor prognosis in many types of cancer, including breast, pancreatic ductal, liver hepatocellular, sarcoma, kidney renal clear cell, and uterine corpus endometrial cancer. In head and neck cancer, the difference was not statistically significant but aligned in a similar trend with other cancers (**Supplementary Figure 4**). These data further indicated that PSAT1 is associated with cancer progression in multiple types of cancers.

Next, we confirmed the contribution of PSAT1 to EV secretion in other cancer types. We cultured a variety of cancer cell lines, such as ovarian (A2780, ES2, and SKOV3), breast (MDA-MB-231), melanoma (A375), head and neck (HSC3), multiple myeloma (RPMI8226), and pancreatic (Panc-1) cell lines. EVs secreted from these cells were collected by ultracentrifugation after PSAT1 siRNA transfection. EV particle number was decreased in all cell lines after PSAT1 silencing **(Figure 5e)**. Although we did not observe a significant difference in PSAT1 expression between normal and cancer cells in pancreatic cancer **(Figure 5c, bottom right)**, the particle number in Panc-1 cells was clearly decreased after PSAT1 silencing **(Figure 5e)**. The data suggested that PSAT1 positively regulates EV secretion in multiple types of cancer.

Increased EV secretion by PSAT1 in breast cancer enhanced osteoclast differentiation

During the expression analyses of PSAT1 in a number of cancer cell lines, we observed higher expression of PSAT1 in metastatic breast cancer cell lines than in their parental cell lines **(Figure 6a**). The bone metastatic cell line BM022 (**Figure 6a, top panels**) and lymph node metastatic cell

line D3H2LN (**Figure 6a, bottom panels**) produced greater amounts of PSAT1 protein than their parental cell lines MCF7 and MDA-MB-231, respectively. We also found that metastatic cell lines secreted higher amounts of EVs than parental cells (**Figure 6b**). To investigate the effect of PSAT1 in bone metastatic breast cancer cells, we established stable clones of PSAT1 overexpression from MCF7 and BM022 cells (**Supplementary Figure 5a**). All PSAT1-overexpressing cells, except for one MCF7 clone, were resistant to serine depletion (**Supplementary Figure 5b**). Enhanced expression of PSAT1 significantly increased the amount of EVs secreted from BM022 cells (**Figure 6c**). Because BM022 cells have bone metastatic ability, we investigated whether BM022-derived EVs influence osteoclast differentiation. Using a Boyden chamber coculture system, osteoclast differentiation of RAW 264.7 cells was examined by TRAP (tartrate-resistant acid phosphatase) staining (**Figure 6d**). As shown in **Figure 6e**, PSAT1-overexpressing breast cancer cells with soluble RANKL (sRANKL) treatment significantly induced osteoclast differentiation. Osteoclast differentiation was also stimulated by supplementing of BM022-derived EVs collected with a conventional ultracentrifugation method (**Figure 6f**). Western blot analysis confirmed that PSAT1 overexpression did not increase the RANKL protein level in breast cancer cells or EVs (**Supplementary Figure 5c, top panels**); thus, BM022-derived EVs, whose secretion was induced by PSAT1, might have other effects. We confirmed that PSAT1 overexpression did not influence the particle size of EVs, merely indicating that the enhanced osteoclast differentiation is due to the increased amount of EVs secreted (**Figure 6g**). Additionally, overexpression of PSAT1 did not obviously change EV marker levels (**Supplementary Figure 5c, bottom panels**). These data suggested that PSAT1 promotes EV secretion and indirectly induces osteoclast differentiation via EVs in a bone metastatic breast cancer cell line.

Enhanced PSAT1 expression contributes to bone metastasis of breast cancer

Finally, we sought to investigate whether PSAT1-controlled EV secretion influences bone metastasis in vivo. We utilized a bone metastasis model established by caudal artery injection of BM022 cells (23), and metastatic processes were monitored over time with an in vivo imaging system (IVIS) (**Figure 7a**). In vivo imaging revealed that PSAT1-overexpressing BM022 cells (the bulk population after transduction) significantly promoted bone metastasis (**Figure 7b, c**). A similar trend was also observed using a PSAT1-overexpressing BM022 cell clone (clone #1, **Supplementary Figure 6**). Computed tomography clearly showed an abnormal bone structure in mice injected with PSAT1-overexpressing BM022 cells (**Figure 7d**). Histological investigation indicated marked invasion of BM022 cells into the bone and structural destruction (**Figure 7e**). Consistent with the increased osteoclast differentiation observed in vitro, increased osteoclast differentiation in bone from mice injected with PSAT1-overexpressing BM022 cells was observed by TRAP staining. Unexpectedly, bone formation by osteoblasts, which are stained by alkaline phosphatase (ALP), was also increased in the PSAT1-overexpressing group, presumably due to osteoblast-osteoclast interactions. Overall, our study revealed novel mechanisms of EV secretion via PSAT1-related serine synthesis in multiple types of cancer. In addition, PSAT1-overexpresssing breast cancer cell lines enhanced facilitate bone metastasis by activating osteoclast differentiation.

Discussion

Cancer-derived EVs exacerbate cancer malignancy through modulating microenvironmental cells to tumor-supportive (24-25), stimulate invasion and metastasis (26-27), and drug resistance (6, 28-29). Therefore, intervening transfer of cancer-derived EVs is expected to be a new therapeutic strategy for cancer (30-31). In this study, we identified miR-891b as a microRNA decreasing EV secretion in cancer through downregulating PSAT1, an enzyme catalyzes serine synthesis. Additionally, PSAT1 is associated with cancer progression in multiple types of cancers. The results using metastatic breast cancer cell lines revealed that PSAT1-controlled EV secretion might facilitate bone metastasis by activating osteoclast differentiation.

Our results showed that higher expression of PSAT1 in cancer cells may explain higher expression of EVs by cancer cells than normal cells. Serine-related metabolic pathways enhance cancer cell proliferation (32-34). HCT116 cells is highly dependent on de novo biosynthesis of serine and glycine (33, 35). Serine is also known to be critical for survival and growth in cancer cells and has been shown to play a central role in metabolic reprogramming. Serine metabolic pathway is important for synthesis of ceramide, which is one of the EVs component (11). Our results suggested that activation of serine-related pathway may contribute to increase of EVs release by supplying the membrane component of EVs in cancer cells.

In some cancer cells, the copy number of the PHGDH gene, which encodes the enzyme involved in the first step of serine synthesis, was found to be increased due to gene duplication (36-37). Increased PHGDH expression resulted in morphological abnormalities in mammary epithelial cells (37). Previous studies indicates that abnormal serine metabolism is linked with cancer development and tumor initiation. PSAT1 catalyzes 3-hydroxypyruvate to phosphoserine reaction and also converts glutamine to alpha-ketoglutarate (α-KG), one of the molecules consisting tricarboxylic acid cycle (TCA cycle). Hwang IY et al. showed that PSAT1 is involved

in maintaining intracellular α-KG levels in both cancer and normal cells (38). In addition, PSAT1 is associated with vitamin B6 metabolism (39-40). One of the target genes of miR-891b other than PSAT1 that was involved in EV secretion was PDXK, which is associated with vitamin B6 metabolism. Silencing of PDXK with siRNA decreased EV secretion **(Supplementary Figure 2)**. Thus, vitamin B6 metabolism may also be involved in EV secretion together with the serine synthesis pathway. We showed that miR-891b regulates EV secretion via multiple pathways, it is because that miRNAs posttranscriptionally regulate the expression of a large number of genes (41). Focusing not on a single pathway but on the whole network of processes becomes important when considering cancer progression.

In this study, we provide evidence that PSAT1-controlled EV secretion promotes osteoclast differentiation, presumably leading to bone metastasis in vivo. Although the precise molecular mechanism by which cancer EVs promote osteoclast differentiation is still unknown, targeting EV secretion could be a promising therapeutic strategy for preventing metastasis. Therefore, one of the optimal target pathways is serine synthesis, and several chemical compounds, such NCT-503, a PHGDH inhibitor (42-43), and fumonisin B1, a ceramide synthesis inhibitor (44), are available for targeting the serine-ceramide synthesis pathway; in addition, GW4869, a well-known EV secretion inhibitor targeting nSMase2 (3) is available. The utility of these chemical compounds may make them a more reasonable and feasible strategy for clinical application than genetic approaches such as siRNA administration.

This study has limitations. First, the ExoScreen method in the presented study could detect the CD63 or CD9 positive-small EVs; therefore, the small EVs without these marker genes are not detected. Further analysis is needed to evaluate the relationship between CD63 or CD9-negative small EVs and the serine synthesis pathway. Second, we showed the increase of EVs release in several types of cancer; however, we did not evaluate the cargo of sEVs derived from

PSAT1-related pathway. In osteoclast differentiation in vitro, the sEVs derived from MCF7-BM022 expressing PSAT1 cells enhanced more differentiated osteoclasts compare to the sEVs derevied from MCF7-parent expressing PSAT1 cells. It means that the cargo derived from metastatic breast cancer cell lines has the potential to enhance the differentiation; therefore, analysis of the cargo is an issue for further evaluation.

In summary, our study revealed novel mechanisms of EV secretion via PSAT1-related serine synthesis in multiple types of cancer. In addition, our studies in an in vivo model of metastatic breast cancer revealed that PSAT1-controlled EV secretion might facilitate bone metastasis by activating osteoclast differentiation. These findings may provide a novel cancer treatment strategy through targeting of serine synthesis.

Materials and Methods

Cell culture

HCT116, HCT15, COLO201, COLO205, CCD-18co, A549, H1650, H2228, A427, HBEC, RPMI8226, A375, Panc-1, HSC3, HSC4, A2780, SKOV3, ES2, SCC25, MCF-7, and MDA-MB-231 cells were purchased from ATCC (American Type Culture Collection, USA). The metastatic MDA-MB-231 cell line D3H2LN was purchased from Xenogen. Bone metastatic cells (BM022) were generated from MCF-7 cells (45). Cells were cultured in Dulbecco's modified Eagle's medium (DMEM) and RPMI 1640 medium (Gibco, USA) supplemented with 10% fetal bovine serum (FBS) and 1% antibiotic-antimycotic (Gibco, USA), and all cells were maintained in an atmosphere of 95% air and 5% CO_2. Normal human epithelial cells were cultured in keratinocyte-SFM medium (Gibco, USA) supplemented with 1% antibiotic-antimycotic (Gibco, USA).

Reagents

The following antibodies were used for ExoScreen analysis: mouse monoclonal anti-human CD9 (clone 12A12, Cosmo Bio, Japan) and anti-human CD63 (clone 8A12, Cosmo Bio, Japan). These antibodies were used to modify either acceptor beads or biotin following the manufacturer's protocol. The following miRNA mimics and siRNAs were purchased from Ambion (USA) and were used for the transient transfection assay: miR-891b mimic (4464066), miRNA Mimic Negative Control #1 (4464058), Rab27a siRNA (S11693), Rab27b siRNA (S11697), and nSMase2 siRNA (S30925). Allstar negative control siRNA (SI03650318) and TSG101 siRNA (SI02655184) were purchased from Qiagen (Hilden, Germany). PSAT1 siRNA (siGENOME SMARTpool siRNA M-010398), PHGDH siRNA (siGENOME SMARTpool siRNA M-009518) and PSPH siRNA (siGENOME SMARTpool siRNA M-011888) were purchased from

Dharmacon (USA). Serine was purchased from Sigma–Aldrich for the serine supplementation experiment.

EV isolation

Cancer cells were seeded in normal medium and cultured for 24 hours, and the medium was then replaced with serum-free advanced DMEM medium supplemented with 2 mM L-glutamine and 1% antibiotic-antimycotic (Gibco, USA). After incubation for 48 hours, the conditioned medium was filtered with a 0.22 μm filter (Millipore, USA) and centrifuged at 2,000 × g for 10 min to remove cell debris. For EV preparation, the conditioned medium was ultracentrifuged at 110,000 × g for 70 min at 4 °C. The EV protein concentration was measured by using a Micro BCA Protein Assay Kit (Thermo Scientific, USA). The collection method, validation, and quantification methods suffice the MISEV2018 guidelines (46).

Western blot analysis

The following antibodies were used as primary antibodies: mouse monoclonal anti-human CD9 (clone 12A12, dilution 1:1000) and anti-human CD63 (clone 8A12, dilution 1:1000) from Cosmo Bio (Japan). The rabbit polyclonal anti-human PSAT1 antibody (10501-1-AP, dilution 1:200) was purchased from Proteintech Group. Mouse anti-actin and rabbit monoclonal anti-human EEA1 and anti-human Rab7 antibodies were purchased from Abcam. Secondary antibodies (horseradish peroxidase-conjugated anti-mouse IgG, NA931, or horseradish peroxidase-conjugated anti-rabbit IgG, NA934; dilution 1:5000) were purchased from GE Healthcare., The same amount of protein was loaded in each lane of Mini-PROTEAN TGX gels (4–20%, Bio–Rad, USA). The antibody signals were detected by chemiluminescence using ImmunoStar LD

(Wako, Japan), and analyzed by a luminescence imaging system (LAS-4000; Fujifilm Inc., Japan).

miRNA-based screening using the ExoScreen assay system

miRNA-based screening was performed as described previously (14). In brief, cancer cells (5×10^3 cells) were seeded in 96-well plates in DMEM supplemented with 10% FBS and 1% antibiotic-antimycotic (Gibco, Japan). After 24 hours of incubation, the AccuTarget™ Human miRNA Mimic Library, which was constructed based on miRBase ver. 21 (CosmoBio, Japan), was transfected into the cells with DharmaFECT Transfection Reagent 1 (Dharmacon, USA). The transfected cells were cultured in serum-free advanced DMEM. After 48 hours, an ExoScreen assay (21) was performed. The plate was read on an EnSpire Alpha 2300 Multilabel Plate Reader at an excitation wavelength of 680 nm and emission wavelength of 615 nm. Background signals obtained from filtered advanced RPMI medium or PBS were subtracted from the measured signals.

Cell proliferation assay

Cell viability was determined using a Cell Counting Kit-8 (Dojindo, Japan) according to the manufacturer's instructions, and the absorbance at 450 nm was measured using an EnVision Multilabel Plate Reader (PerkinElmer, USA).

Nanoparticle tracking analysis

EVs were resuspended in PBS and further diluted for analysis with a NanoSight LM10-HS system according to the manufacturer's protocol.

RNA Extraction and Microarray Analysis

A microarray analysis was performed as described previously (10). Total RNA was extracted from cultured cells using QIAzol reagent and a miRNeasy Mini Kit (Qiagen, Germany). RNA quantity and quality were determined using a NanoDrop ND-1000 spectrophotometer (Thermo Fisher, USA) and an Agilent Bioanalyzer (Agilent Technologies, USA).

Quantitative real-time polymerase chain reaction

Total RNA was extracted from cultured cells using QIAzol reagent and a miRNeasy Mini Kit (Qiagen, Germany). RNA quantity and quality were determined using a NanoDrop ND-1000 spectrophotometer (Thermo Fisher, USA). For qRT–PCR analysis, complementary DNA was generated from total RNA using a High Capacity cDNA Reverse Transcription Kit (Applied Biosystems, USA). The data were collected and analyzed using StepOne software v2.3 (Applied Biosciences, USA). All quantitative mRNA expression data were normalized to the expression of β-actin. TaqMan probes for PSAT1 and β-actin were purchased from Applied Biosystems.

Luciferase reporter assay plasmid construction

A 1015 base pair fragment from the 3'UTR of PSAT1 containing the predicted target sequences of miR-891b (located from base pair 317 to base pair 327) was generated. The following annealed oligos, including the predicted target sequences of miR-891b (Thermo Fisher, USA), were used to construct 3'UTR reporter vectors. PSAT1_3UTR_S: 5'TCGAGAGTTAGATTTCAAACTTGCCTGTGGACTTAATAATGCAAGTTGCGATTAATTATTTCTGGAGTCATGGGAACACGC3'; PSAT1_3UTR_AS: 5'GGCCGCGTGTTCCCATGACTCCAGAAATAATTAATCGCAACTTGCATTATTAAGTCCACAGGCAAGTTTGAAATCTAACTC3'; PSAT1_mut_3UTR_S:

5'TCGAGAGTTAGATTTCAAACTTGCCTGTGGACTTAATAATGCTTCAACGGATTAA TTATTTCTGGAGTCATGGGAACACGC3'; and PSAT1_mut_3UTR_AS: 5'GGCCGCGTGTTCCCATGACTCCAGAAATAATTAATCCGTTGAAGCATTATTAAGT CCACAGGCAAGTTTGAAATCTAACTC3'. Annealed oligos were ligated into the Xho I and Not I sites in the 3'UTR of the Renilla luciferase gene in the psiCHECK-2 plasmid (Promega, USA). Each plasmid was cotransfected into HEK 293 cells with miR-891b using Dharmafect 1 Transfection Reagent (Dharmacon, USA). Cells were cultured for 48 hours after transfection; then, firefly luciferase activity was measured and normalized to Renilla luciferase activity.

Immunofluorescence

Cancer cells (1×10^5) were seeded into 35 mm uncoated glass dishes. After 24 hours of incubation, siPSAT1 and Allstar negative control siRNA were transfected into each cell line, and after another 24 hours of incubation, the medium was changed to serum-free advanced DMEM. Confocal microscopy was performed with an Olympus FV10i laser scanning microscope. The same primary antibodies as western blotting were used. Secondary antibodies conjugated to the following fluorophores were used: Alexa Fluor 405 (for Hoechst 33442), Alexa Fluor 488 (for PSAT1, EEA1, Rab7), and Alexa Fluor 594 (for CD63).

Serine depletion experiment and inhibition of the serine synthesis pathway

MEM supplemented with 1 × insulin, transferrin, selenium solution (ITS-G, 100X), and 1 × MEM vitamin solution (100X), with or without serine (4 mM), was used for serine depletion experiments. Cancer cells were seeded into 96-well plates (5×10^3 cells) or 6-well plates (1.5×10^5 cells) and were then incubated for 24 hours. Then, siPSAT1 and Allstar negative control siRNA were transfected into each cell line. After 24 hours of incubation, the medium was changed

to serum-free modified MEM. After another 48-hour incubation, the 96-well plates were used for the ExoScreen assay, and conditioned medium was collected from the 6-well plates. EVs were isolated from the conditioned medium, and NTA was then conducted. The rate of EV secretion inhibition was calculated based on the ExoScreen assay data and was normalized to the cell proliferation assay data.

In silico analysis and expression analysis of PSAT1

Candidate miR-891b target genes were predicted with the TargetScan database (http://www.targetscan.org/cgi-bin/targetscan/vert_72/targetscan.cgi?species=Human&gid=&mir_sc=&mir_c=&mir_nc=&mir_vnc=&mirg=mir-891b). PSAT1 expression data from cancer tissues and normal tissues were obtained from the Oncomine database (https://www.oncomine.org/resource/login.html). Salamat lung data (N=116) and Gaedcke colorectal data (N=130) were used for reanalysis. Overall survival data were obtained from the Kaplan–Meier plotter database (https://kmplot.com/analysis/index.php?p=service&cancer=lung).

Osteoclast differentiation & TRAP staining

RAW264.7 cells, a mouse macrophage cell line (ATCC), were cultured in minimum essential medium alpha (MEM-α) (Gibco) containing 10% fetal bovine serum (FBS) and 1% antibiotic-antimycotic (Gibco, USA) and were maintained in an atmosphere of 95% air and 5% CO_2. To generate osteoclasts, RAW264.7 cells were cultured for 72 hours in the presence of 50 ng/mL RANKL (47187000, ORIENTAL YEAST CO. LTD.). Osteoclast differentiation was measured with a Tartrate-Resistant Acid Phosphatase (TRAP) Assay Kit (AK04F, Cosmo Bio). Stained cells with three or more nuclei were counted as TRAP-positive.

Generation of PSAT1 OE cells

MCF-7 and BM022 cells (1 x 10^5 cells) were seeded into 24-well dishes, and the PSAT1 overexpression vector (RC202475, Origene) was transfected by using Lipofectamine LTX Plus reagent (15338-100, Thermo Fisher). After 24 hours, cells were transferred to 150 cm^2 dishes containing 500 ng/mL geneticin (10131-027, Gibco). After geneticin selection, colonies were picked and transferred to new dishes. Cells that grew were established as PSAT1-overexpressing cells. The protein level of PSAT1 was validated by Western blotting.

In vivo experiments

Female NOD.CB-17-Prkdc<scid>/J mice (NOD/scid, Charles River Japan, Inc.) were used for the animal study. After anesthetization of the mice with isoflurane gas, PSAT1-overexpressing BM022 cells (1 x 10^6 cells/100 μL in PBS (-) solution) were injected through the caudal artery. Bone metastasis was monitored every week by bioluminescence using an IVIS imaging system. Mice were sacrificed 28 days after transplantation.

Statistical analysis

The data presented in the bar graphs are the means ± SE of at least three independent experiments. Differences between two groups were analyzed by Student's t test. Differences with $p<0.05$ were considered to be statistically significant. One-way analysis of variance (ANOVA) followed by Tukey's honestly significant difference (HSD) post hoc test for multiple comparisons was used to determine the significance of differences among three groups. For multiple comparisons, the significance of differences in the average values was analyzed using one-way ANOVA with Dunnett's post hoc test.

Author contributions

TY, JN and FU designed the study. TY, KI and YY performed experiments. TY, YY, MK and YH analyzed data. YY and TO wrote the manuscript.

Acknowledgement

We thank M. Abe and N. Nishida-Aoki for the support on this study. This study was supported by the Practical Research for Innovative Cancer Control (19ck0106366h0003) from the Japan Agency for Medical Research and Development (AMED); MEXT KAKENHI (Grant-in-Aid for Scientific Research (B): 21H02721; Princess Takamatsu Cancer Research Fund; Kobayashi Foundation for Cancer Research; and Novartis Research Grants; Foundation for Promotion of Cancer Research.

References

1. van Niel, G., D'Angelo, G. & Raposo, G. Shedding light on the cell biology of extracellular vesicles. *Nat Rev Mol Cell Biol.* 19, 213-228 (2018).
2. Raposo, G. & Stoorvogel, W. Extracellular vesicles: exosomes, microvesicles, and friends. *J. Cell Biol.* **200**, 373-83 (2013).
3. Kosaka, N. et al. Neutral sphingomyelinase 2 (nSMase2)-dependent exosomal transfer of angiogenic microRNAs regulate cancer cell metastasis. *J. Biol. Chem*. **288**, 10849-59 (2013).
4. Cui, H. et al. Tissue inhibitor of metalloproteinases-1 induces a pro-tumourigenic increase of miR-210 in lung adenocarcinoma cells and their exosomes. *Oncogene* **34**, 3640-3650 (2015).
5. Li, M. Y., Liu, L. Z., & Dong, M. Progress on pivotal role and application of exosome in lung cancer carcinogenesis, diagnosis, therapy and prognosis. *Mol Cancer.* **20**, 22 (2021).
6. Wu, S. et al. Intercellular transfer of exosomal wild type EGFR triggers osimertinib resistance in non-small cell lung cancer. *Mol Cancer*. **20**, 17 (2021).
7. Nishida-Aoki, N. et al. Disruption of Circulating Extracellular Vesicles as a Novel Therapeutic Strategy against Cancer Metastasis. *Mol. Ther.* **25**, 181-91 (2017).
8. Yanez-Mo, M. et al. Biological properties of extracellular vesicles and their physiological functions. *J. Extracell. Vesicles* **4**, 27066 (2015).
9. Cocucci, E. & Meldolesi, J. Ectosomes and exosomes: shedding the confusion between extracellular vesicles. *Trends Cell Biol.* **25**, 364-72 (2015).
10. Vietri, M., Radulovic, M. & Stenmark, H. The many functions of ESCRTs. *Nat Rev Mol Cell Biol.* **21**, 25-42 (2020).

11. Trajkovic, K. et al. Ceramide triggers budding of exosome vesicles into multivesicular endosomes. *Science* **319**, 1244-7 (2008).
12. Matsui, T., Osaki, F., Hiragi, S., Sakamaki, Y. & Fukuda, M. ALIX and ceramide differentially control polarized small extracellular vesicle release from epithelial cells. *EMBO Rep*. **22**, e51475 (2021).
13. Kilinc, S. et al. Oncogene-regulated release of extracellular vesicles. *Dev. Cell* **56**, 1989-2006 (2021).
14. Urabe, F. et al. miR-26a regulates extracellular vesicle secretion from prostate cancer cells via targeting SHC4, PFDN4 and CHORDC1. *Sci. Adv.* **6**, 18, eaay3051 (2020).
15. Urabe, F. et al. The miR-1908/SRM regulatory axis contributes to extracellular vesicle secretion in prostate cancer. *Cancer Sci.* **111**, 3258-3267 (2020).
16. Ruan, Z. et al. P2RX7 inhibitor suppresses exosome secretion and disease phenotype in P301S tau transgenic mice. *Mol Neurodegener.***15**, 47 (2020).
17. Kosaka, N. et al. Competitive interactions of cancer cells and normal cells via secretory microRNAs. *J. Biol. Chem.* **287**, 1397-405 (2012).
18. O'Brien K, Breyne K, Ughetto S, Laurent LC, Breakefield XO. RNA delivery by extracellular vesicles in mammalian cells and its applications. *Nat Rev Mol Cell Biol.* **21**, 585-606 (2020).
19. Han, M. et al. Exosome-transmitted miR-567 reverses trastuzumab resistance by inhibiting ATG5 in breast cancer. *Cell Death Dis.* **11**, 43 (2020).
20. Leblanc R, Kashyap R, Barral K, Egea-Jimenez AL, Kovalskyy D, Feracci M, Garcia, M. et al. Pharmacological inhibition of syntenin PDZ2 domain impairs breast cancer cell activities and exosome loading with syndecan and EpCAM cargo. *J Extracell Vesicles.* **10**, e12039 (2020).

21. Yoshioka, Y. Ultra-sensitive liquid biopsy of circulating extracellular vesicles using ExoScreen. *Nat. Commun*. **5**, 3591 (2014).

22. Qian, C.,ia, Y., Ren, Y., Yin, Y & Deng, A. Identification and validation of PSAT1 as a potential prognostic factor for predicting clinical outcomes in patients with colorectal carcinoma. *Oncol. Lett.* **14**, 8014-8020 (2017).

23. Kuchimaru, T. et al. A reliable murine model of bone metastasis by injecting cancer cells through caudal arteries. *Nat. Commun.* **9,** 2981 (2018).

24. Naito, Y. et al. Cancer extracellular vesicles contribute to stromal heterogeneity by inducing chemokines in cancer-associated fibroblasts. *Oncogene* **38**, 5566-5579 (2019).

25. Zhan, X. et al. Hypoxic BMSC-derived exosomal miRNAs promote metastasis of lung cancer cells via STAT3-induced EMT. *Mol Cancer*. **18**, 40 (2019).

26. Yokoi, A. et al. Malignant extracellular vesicles carrying MMP1 mRNA facilitate peritoneal dissemination in ovarian cancer. *Nat. Commun.* **8**, 14470 (2017).

27. Morrissey, S. M. et al. Tumor-derived exosomes drive immunosuppressive macrophages in a pre-metastatic niche through glycolytic dominant metabolic reprogramming. *Cell Metab*. **33**, 2040-2058 (2021).

28. Yamamoto, T. et al. SORT1/LAMP2-mediated extracellular vesicle secretion and cell adhesion are linked to lenalidomide resistance in multiple myeloma. *Blood Adv*. **6**, 2480-2495 (2022).

29. Boelens, M. C. et al. Exosome transfer from stromal to breast cancer cells regulates therapy resistance pathways. *Cell* **159**, 499-513 (2014).

30. Kosaka, N., Yoshioka, Y., Fujita, Y. & Ochiya, T. Versatile roles of extracellular vesicles in cancer. *J Clin Invest*. **126**,1163-72 (2016).

31. Xu, Z., Zeng, S., Gong, Z. & Yan Y. Exosome-based immunotherapy: a promising approach for cancer treatment. *Mol Cancer*. **19**, 160 (2020).

32. DeNicola, G.M. et al. NRF2 regulates serine biosynthesis in non-small cell lung cancer. *Nat Genet*. **47**, 1475-81 (2015).

33. Montrose, D.C. et al., Exogenous and Endogenous Sources of Serine Contribute to Colon Cancer Metabolism, Growth, and Resistance to 5-Fluorouracil. *Cancer Res*. **81**, 2275-2288 (2021).

34. Raines, L.N. et al. PERK is a critical metabolic hub for immunosuppressive function in macrophages. *Nat Immunol*. **23**, 431-445 (2022).

35. Chaneton, B. et al. Serine Is a Natural Ligand and Allosteric Activator of Pyruvate Kinase M2. *Nature* **491**, 458-462 (2012).

36. Possemato, R. et al. Functional Genomics Reveal That the Serine Synthesis Pathway Is Essential in Breast Cancer. *Nature* **476**, 346-350 (2011).

37. Locasale, J. W. et al. Phosphoglycerate Dehydrogenase Diverts Glycolytic Flux and Contributes to Oncogenesis. *Nat. Genet.* **43**, 869-874 (2011).

38. Hwang, I. Y. Psat1-Dependent Fluctuations in α-Ketoglutarate Affect the Timing of ESC Differentiation. *Cell Metab.* **24**, 494-501 (2016).

39. Ramos, R. J. et al. Vitamin B6 is essential for serine de novo biosynthesis. *J. Inherit Metab. Dis.* **40**, 883-891 (2017).

40. Zhang, L. et al. Pyridoxine 5'-phosphate oxidase is a novel therapeutic target and regulated by the TGF-β signalling pathway in epithelial ovarian cancer. *Cell Death Dis.* **8**, 3214 (2017).

41. Ambros, V. The functions of animal microRNAs. *Nature* **431**, 350-5 (2004).

42. Pacold, M. E. et al. A PHGDH inhibitor reveals coordination of serine synthesis and one-carbon unit fate. *Nat. Chem. Biol.* **12**, 452-8 (2016).

43. Issaq, S. H. et al. EWS-FLI1-regulated Serine Synthesis and Exogenous Serine Are Necessary for Ewing Sarcoma Cellular Proliferation and Tumor Growth. *Mol. Cancer Ther.* **19**, 1520-1529 (2020).

44. Tolleson, W. H. et al. Apoptotic and Anti-Proliferative Effects of Fumonisin B1 in Human Keratinocytes, Fibroblasts, Esophageal Epithelial Cells and Hepatoma Cells. *Carcinogenesis* **17**, 239-49 (1996).

45. Han, Y. et al. Establishment and characterization of highly osteolytic luminal breast cancer cell lines by intracaudal arterial injection. *Genes Cells* **25**, 111-123 (2020).

46. Théry, C. et al. Minimal information for studies of extracellular vesicles 2018 (MISEV2018): a position statement of the International Society for Extracellular Vesicles and update of the MISEV2014 guidelines. *J. Extracell. Vesicles* **7**, 1535750 (2018).

Figure legends

Fig. 1 miRNA screening identified miR-891b as being responsible for EV secretion. a. A schematic of miRNA-based screening for EV secretion. **b.** Western blot analysis of the EV surface markers CD9 and CD63 in EV samples collected from HCT116 and A549 cells. EVs were loaded at 500 ng protein/lane. **c.** NTA of EVs from HCT116 and A549 cells. **d.** EV secretion of cancer cells with knock-down of EV secretion-related genes. Left: HCT116, Right: A549. Normalized to NC, negative control; showing the mean ± SEs (n=3). *P < 0.05, the one-way analysis of variance test. **e.** Relative cell viability after introducing miRNA was evaluated with MTS assay. The signals were normalized to those in the negative control group. miRNAs with a signal < 0.8 or > 1.2 were excluded. **f.** Dot plots of EV secretion levels of cancer cells transfected with each miRNA. Top: HCT116, Bottom: A549. Relative EV secretion changes were calculated in Z-scores. Only miRNAs with less impact on cellular viability are shown (0.8 < viability< 1.2). **g.** Top 10 miRNAs with high z-scores of EV secretion.

Fig. 2 Screening of miR-891b target genes. a. Venn diagram showing overlaps among genes downregulated by miR-891b transfection in HCT116 and A549 cells (Fc < -1.5) and target genes of miR-891b predicted by TargetScan. **b.** Schematic of the miR-891b target gene screening. After siRNAs were transfected into HCT116 or A549 cells, secreted EV amount was measured by ExoScreen (both CD9- and CD63-positive) **c.** Heat map showing EV secretion levels of cells with gene silencing. **d.** EV secretion levels after siPSAT1 introduction. EV secretion was measured by the ExoScreen based on the surface CD9 or CD63 levels. The showing the mean ± SE (n = 3). *P < 0.05, the Student's t test. **e.** Nanoparticle tracking analysis of EVs collected from siPSAT1-transfected cancer cells. The particle count was normalized by the cell number, when the

conditioned medium collected. The showing the mean ± SE. *P < 0.05, the Student's t test. **f.** PSAT1 expression levels in miR-891b-transfected cancer cells. The relative expression levels of PSAT1 were normalized to β-actin expression. The values are presented as the means±SEs (n = 3). *, p<0.05. **g.** Western blot analysis of PSAT1 after miR-891b was transfected. Each lane was loaded with 15 μg protein. **h.** Summary of miR-891b target sites and mutated sites (shown in bold) in the 3′UTRs of PSAT1. **i.** The results of the luciferase reporter assay with the wild-type and mutant PSAT1 3'UTR cotransfected with miR-891b. The values are the means ± SE (n = 8, *, p<0.05, Student's t test)

Fig. 3 Investigation of the association between PSAT1 expression and EV biogenesis. a. Co-staining of the nucleus (blue) with PSAT1 (red) and CD63 (green) in PSAT1-silenced cells. **b.** Co-staining of Rab7, a late endosome marker (red), with CD63 (green). **c.** Quantification of sum of the CD63 single-positive area in HCT116 and A549 cells in the PSAT1-silenced and control groups (n = 10, *, p<0.05, Student's t test)

Fig. 4 The de novo serine synthesis pathway affected EV secretion in cancer cell lines. a. Schematic of the serine de novo synthesis pathway. **b.** Schematic for the serine depletion experiments of EVs . **c, d.** Rescue experiments were performed to determine the effect of siPSAT1 with the addition of serine. After transfection with siPSAT1, serine was added to the serine-depleted medium (4 mM). EV secretion was measured by the ExoScreen method. The values are the means ± SE (n = 3). *P < 0.05, the one-way analysis of variance test. **e, f.** NTA of EVs secreted in the rescue experiments with serine addition. The particle count was normalized to the cell count. The values are the means ± SE (n = 3). *, p<0.05. **g, h.** Knock-down of PHGDH and PSPH with each siRNA in HCT116 and A549 cell lines. **i.** Viability of HCT116 and A549 cells after PHGDH

and PSPH silencing. Cell viability was measured with a CCK-8 kit. The values are the means ± SE (n = 3). *, $p<0.05$, the one-way analysis of variance test. **j.** NTA of EVs secreted from HCT116 and A549 cells after PHGDH and PSPH silencing. The values are the means ± SE (n = 3). *, $p<0.05$, the one-way analysis of variance test.

Fig. 5. PSAT1 universally regulates EV secretion in cancer. a. qRT–PCR analysis of the expression level of PSAT1 across colorectal and lung cancer cell lines. Expression levels were normalized to β-actin expression. The values are the means ± SE (n = 3). *, $p<0.05$, the one-way analysis of variance test. **b.** Positive correlation between PSAT1 expression and EV secretion. **c.** Expression levels of PSAT1 between cancer and normal tissues in several types of cancer based on the Oncomine database, Student's t test. **d.** Kaplan–Meier analysis based on PSAT1 expression in lung cancer (all stages, stage I, II and III). **e.** The effect of siPSAT1 on EV secretion across cancer cell lines. EV secretion was measured by NTA. The values are the means ± SE (n = 3). *, $p<0.05$, Student's t test.

Fig. 6. Osteoclast differentiation promoted by PSAT1 controls EV secretion in BM022 metastatic breast cancer cells. a. Western blot analysis of PSAT1 in parental cells (MCF7 and MDA-MB-231) and the corresponding metastatic cells (BM022 and D3H2LN). **b.** Relative EV secretion levels in parental and metastatic cell lines. The number of EVs secreted was normalized to the cell number. The values are the means ± SE (n = 3). *, $p<0.05$, Student's t test. **c.** Relative EV secretion levels in PSAT1-overexpressing cells. The values are the means ± SE (n = 3). *, $p<0.05$, Student's t test. N.S. = not significant. **d.** Diagram of the strategy for evaluating the effect of BM022-derived EVs on osteoclast differentiation of RAW 264.7 cells in a Boyden chamber system. Osteoclast differentiation was evaluated by TRAP staining. **e.** Number of TRAP-positive

cells among PSAT1-overexpressing cells treated with sRANKL. The values are the means ± SE (n = 10, *, $p<0.05$, the one-way analysis of variance test). **f.** Number of TRAP-positive cells after the addition of EVs collected from PSAT1-overexpressing BM022 cells. The values are the means ± SE (n =10, *, $p<0.05$, the one-way analysis of variance test). **g.** NTA was performed to compare particle sizes between PSAT1-overexpressing BM022 cells and control cells. N.S. = not significant.

Fig. 7. PSAT1 overexpression facilitates bone metastasis in a breast cancer model. a. Scheme for establishment of the in vivo bone metastasis model via caudal artery injection. The bulk cell populations of PSAT1-overexpressing BM022 and control cells were used for this in vivo study. **b.** Representative IVIS images of mice injected with PSAT1-overexpressing BM022 and control cells on Days 0, 7, and 28. **c.** Relative luminescence intensity of BM022 cells, which express a luciferase construct, in mice injected with PSAT1-overexpressing BM022 and control cells. *, $p<0.05$. **d.** Computed tomography of bones in mice injected with PSAT1-overexpressing BM022 and control cells. **e-g** Images of HE staining (**e**), TRAP staining (**f**) and ALP staining (**g**) in bone from mice injected with PSAT1-overexpressing BM022 and control cells. Mice were sacrificed on Day 28 after IVIS imaging.

Supplementary Information

Supplementary Table 1. Overlapped 82 genes in Figure 2a.

Supplementary Figure 1. Screening of miRNAs in HCT116 and A549 cells. **a.** Second screen of selected miRNAs in HCT116 and A549 cells. EV secretion was measured by the ExoScreen method. Signals were normalized to the CCK-8 cell viability assay data. **b.** The effect of the miR-891b mimic on EV secretion was evaluated in conditioned medium (CM) and purified EVs. The amount of secreted EVs per cell was evaluated by the signal intensity measured in the ExoScreen assay. The values are presented as the means±SEs (n=3). *, $p<0.05$. Student's t test. **c.** Nanoparticle tracking analysis. The particle count was normalized to the cell count. *, $p<0.05$. Student's t test **. d.** Kaplan–Meier analysis based on miR-891b expression in rectal and lung cancer (https://kmplot.com/analysis/).

Supplementary Figure 2. Other candidate target genes of miR-891b. a. PDXK, RAB31, and VPS37B were downregulated by the corresponding siRNAs (final concentration: 10 nM). The EV secretion level was evaluated by the ExoScreen method. **b.** NTA was used to determine the EV amount after PDXK, RAB31, and VPS37B siRNA transfection. Signals were normalized according to the corresponding cell counts.

Supplementary Figure 3. Effects of miR-891b or PSAT1 silencing on EV biogenesis. a. Costaining of the nucleus (blue) with PSAT1 (red) and CD63 (green) in miR-891b-transfected cells. **b.** Costaining of EEA1, an early endosome marker (red), with CD63 (green). **c.** Costaining of Rab7, a late endosome marker (red), with CD63 (green).

Supplementary Figure 4. Kaplan–Meier analysis based on PSAT1 expression across cancer types. Kaplan–Meier plots (https://kmplot.com/analysis/) by cancer type, including breast, pancreatic ductal, hepatocellular, sarcoma, renal clear cell, uterine corpus endometrial, and head and neck cancer.

Supplementary Figure 5. Establishment of PSAT1-overexpressing cell lines. a. Morphological observation of the MCF7 parental cell line and the BM022 metastatic cell line after PSAT1 overexpression. The increase in PSAT1 protein expression was confirmed by Western blotting (three clones each from MCF7 and BM022 cells). **b.** Serine depletion experiments using PSAT1-overexpressing cell lines. The values are the means ± SE (n = 3). *, $p<0.05$, Student's t test. **c.** Western blot analysis of RANK and RANKL in cells (top panels) and of EV markers such as CD9, CD63, and FLOT-1 in EVs (bottom panels) in PSAT1-overexpressing cell lines.

Supplementary Figure 6. In vivo bone metastasis experiment using PSAT1-overexpressing BM022 (clone #1) cells. a. Representative IVIS images of PSAT1-overexpressing BM022 (clone #1 from **Supplementary Figure 5a**) and control cells on Days 0, 7, and 28. **b.** Relative luminescence intensity of BM022 (clone #1) and control cells on Days 14, 21, and 28. *, $p<0.05$.

Fig. 1

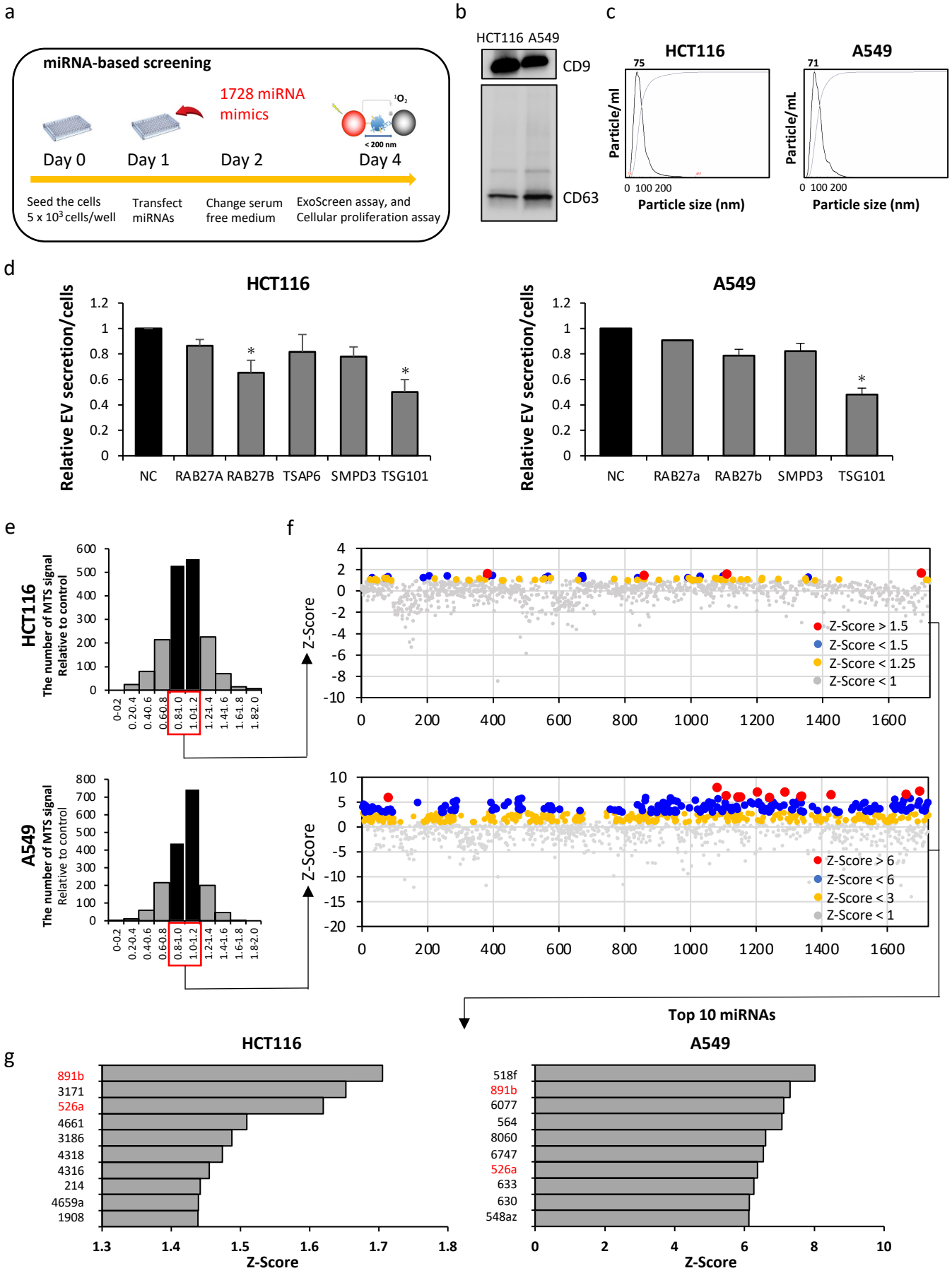
a
miRNA-based screening
1728 miRNA mimics
Day 0
Day 1
Day 2
Day 4
< 200 nm
Seed the cells 5 x 10³ cells/well
Transfect miRNAs
Change serum free medium
ExoScreen assay, and Cellular proliferation assay
b
HCT116 A549
CD9
CD63
c
HCT116
A549
Particle/ml
Particle size (nm)
d
HCT116
A549
Relative EV secretion/cells
NC
RAB27A
RAB27B
TSAP6
SMPD3
TSG101
RAB27a
RAB27b
e
HCT116
A549
The number of MTS signal Relative to control
f
Z-Score
Z-Score > 1.5
Z-Score < 1.5
Z-Score < 1.25
Z-Score < 1
Z-Score > 6
Z-Score < 6
Z-Score < 3
Z-Score < 1
Top 10 miRNAs
g
HCT116
891b
3171
526a
4661
3186
4318
4316
214
4659a
1908
A549
518f
891b
6077
564
8060
6747
526a
633
630
548az
Z-Score

Fig. 2

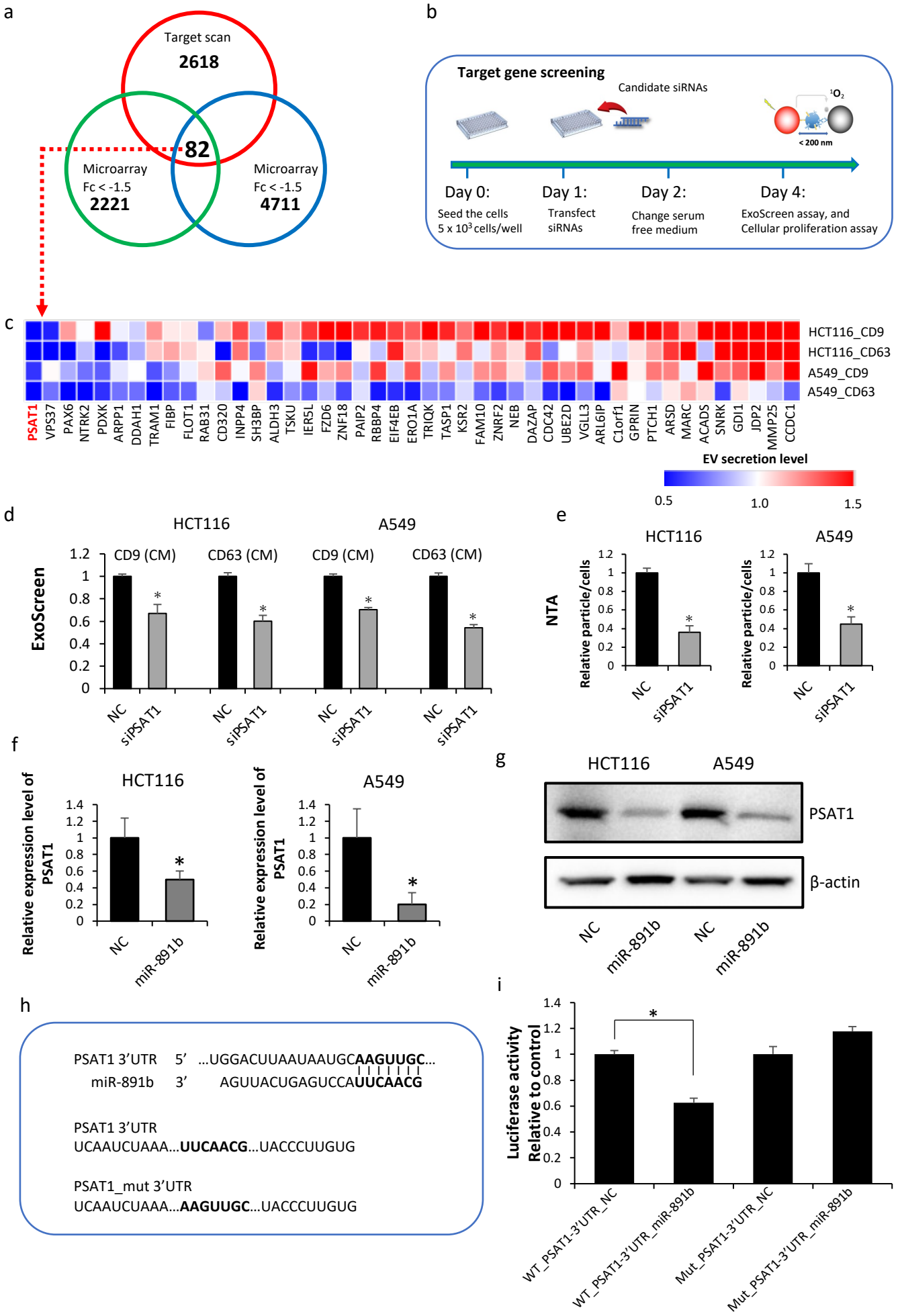
a
Target scan
2618
82
Microarray
Fc < -1.5
2221
Microarray
Fc < -1.5
4711
b
Target gene screening
Candidate siRNAs
< 200 nm
Day 0:
Seed the cells
5 x 10³ cells/well
Day 1:
Transfect
siRNAs
Day 2:
Change serum
free medium
Day 4:
ExoScreen assay, and
Cellular proliferation assay
c
HCT116_CD9
HCT116_CD63
A549_CD9
A549_CD63
PSAT1
VPS37
PAX6
NTRK2
PDXK
ARPP1
DDAH1
TRAM1
FIBP
FLOT1
RAB31
CD320
INPP4
SH3BP
ALDH3
TSKU
IER5L
FZD6
ZNF18
PAIP2
RBBP4
EIF4EB
ERO1A
TRIQK
TASP1
KSR2
FAM10
ZNRF2
NEB
DAZAP
CDC42
UBE2D
VGLL3
ARL6IP
C1orf1
GPRIN
PTCH1
ARSD
MARC
ACADS
SNRK
GDI1
JDP2
MMP25
CCDC1
EV secretion level
0.5
1.0
1.5
d
HCT116
A549
ExoScreen
CD9 (CM)
CD63 (CM)
CD9 (CM)
CD63 (CM)
NC
siPSAT1
e
HCT116
A549
NTA
Relative particle/cells
NC
siPSAT1
f
HCT116
A549
Relative expression level of PSAT1
NC
miR-891b
g
HCT116
A549
PSAT1
β-actin
NC
miR-891b
h
PSAT1 3'UTR 5' ...UGGACUUAAUAAUGCAAGUUGC...
miR-891b 3' AGUUACUGAGUCCAUUCAACG
PSAT1 3'UTR
UCAAUCUAAA...UUCAACG...UACCCUUGUG
PSAT1_mut 3'UTR
UCAAUCUAAA...AAGUUGC...UACCCUUGUG
i
Luciferase activity
Relative to control
WT_PSAT1-3'UTR_NC
WT_PSAT1-3'UTR_miR-891b
Mut_PSAT1-3'UTR_NC
Mut_PSAT1-3'UTR_miR-891b

Fig. 3

a

CD63 PSAT1 Nucleus Merge

HCT116 NC

HCT116 siPSAT1

A549 NC

A549 siPSAT1

(10 µm)

b

NC siPSAT1

HCT116

A549

CD63 Rab7

(10 µm)

c

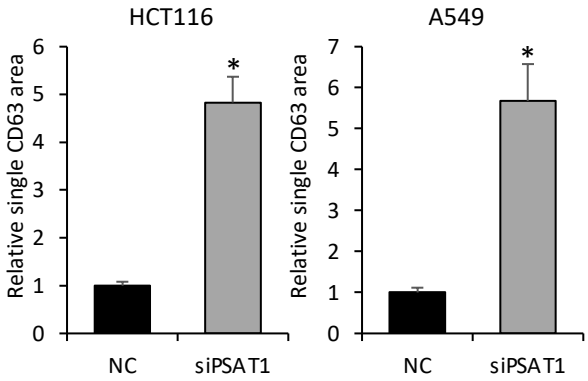

Fig. 4

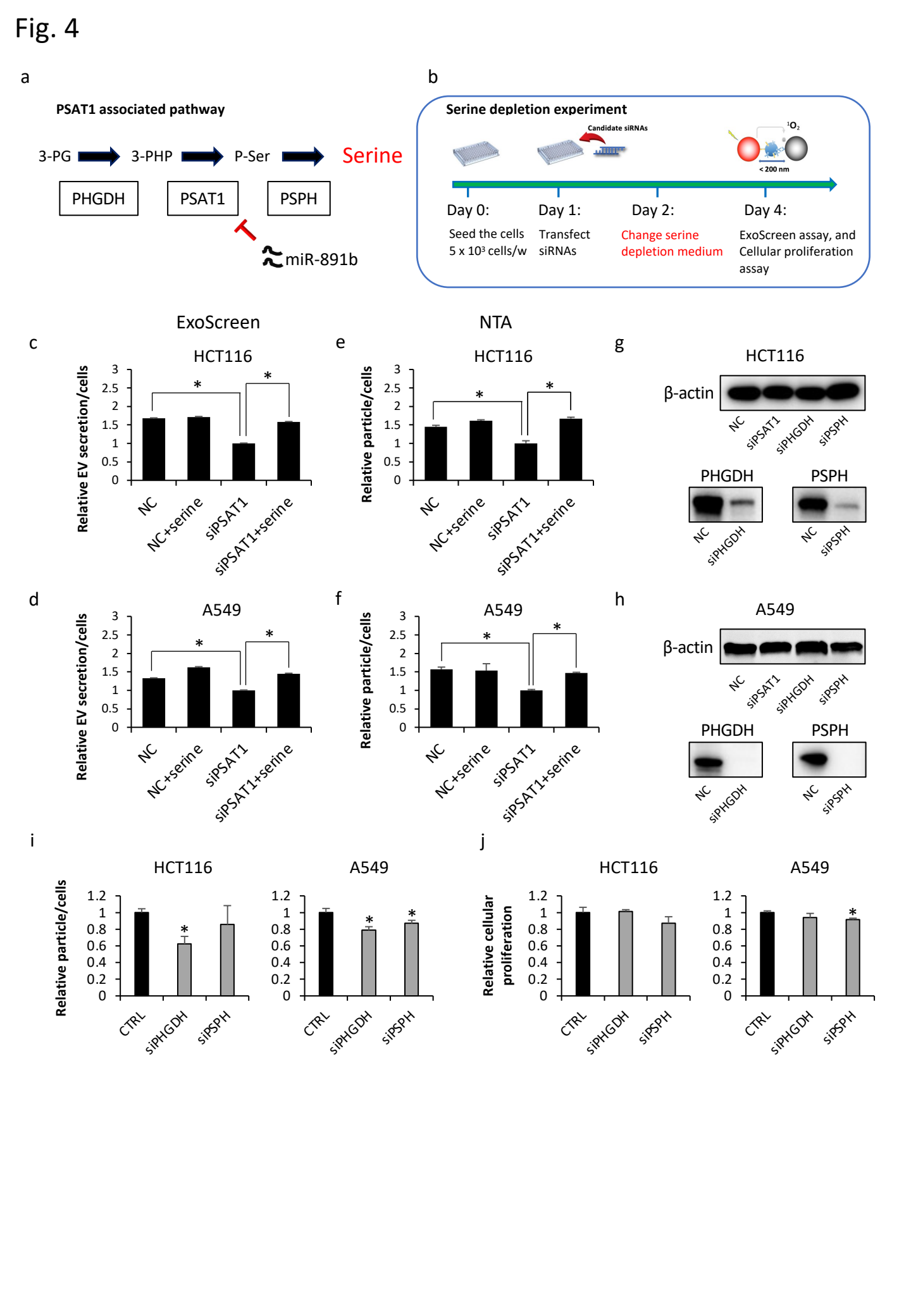
a
PSAT1 associated pathway
3-PG
3-PHP
P-Ser
Serine
PHGDH
PSAT1
PSPH
miR-891b
b
Serine depletion experiment
Candidate siRNAs
$^1O_2$
< 200 nm
Day 0:
Seed the cells
5 x 10³ cells/w
Day 1:
Transfect
siRNAs
Day 2:
Change serine
depletion medium
Day 4:
ExoScreen assay, and
Cellular proliferation
assay
ExoScreen
NTA
c
HCT116
Relative EV secretion/cells
NC
NC+serine
siPSAT1
siPSAT1+serine
e
HCT116
Relative particle/cells
g
HCT116
β-actin
NC
siPSAT1
siPHGDH
siPSPH
PHGDH
PSPH
d
A549
f
A549
h
A549
i
HCT116
A549
Relative particle/cells
CTRL
siPHGDH
siPSPH
j
Relative cellular proliferation

Fig. 5

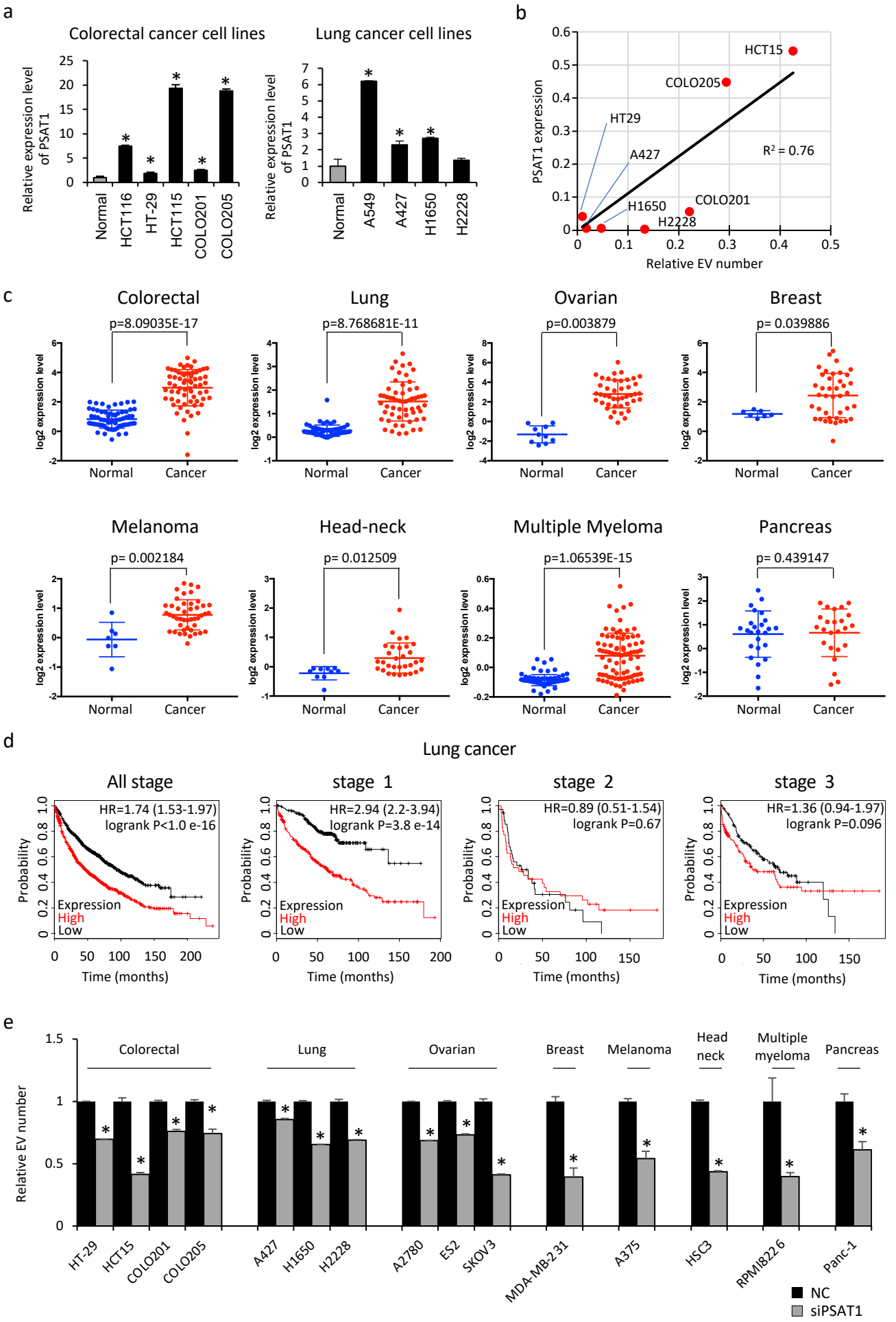
a
Colorectal cancer cell lines
Lung cancer cell lines
Relative expression level of PSAT1
Normal
HCT116
HT-29
HCT115
COLO201
COLO205
A549
A427
H1650
H2228
b
PSAT1 expression
Relative EV number
HCT15
COLO205
HT29
A427
H1650
COLO201
H2228
R² = 0.76
c
Colorectal
p=8.09035E-17
Lung
p=8.768681E-11
Ovarian
p=0.003879
Breast
p= 0.039886
Melanoma
p= 0.002184
Head-neck
p= 0.012509
Multiple Myeloma
p=1.06539E-15
Pancreas
p= 0.439147
log2 expression level
Normal
Cancer
d
Lung cancer
All stage
HR=1.74 (1.53-1.97)
logrank P<1.0 e-16
stage 1
HR=2.94 (2.2-3.94)
logrank P=3.8 e-14
stage 2
HR=0.89 (0.51-1.54)
logrank P=0.67
stage 3
HR=1.36 (0.94-1.97)
logrank P=0.096
Probability
Expression
High
Low
Time (months)
e
Relative EV number
Colorectal
Lung
Ovarian
Breast
Melanoma
Head neck
Multiple myeloma
Pancreas
HT-29
HCT15
COLO201
COLO205
A427
H1650
H2228
A2780
ES2
SKOV3
MDA-MB-231
A375
HSC3
RPMI8226
Panc-1
NC
siPSAT1

Fig. 6

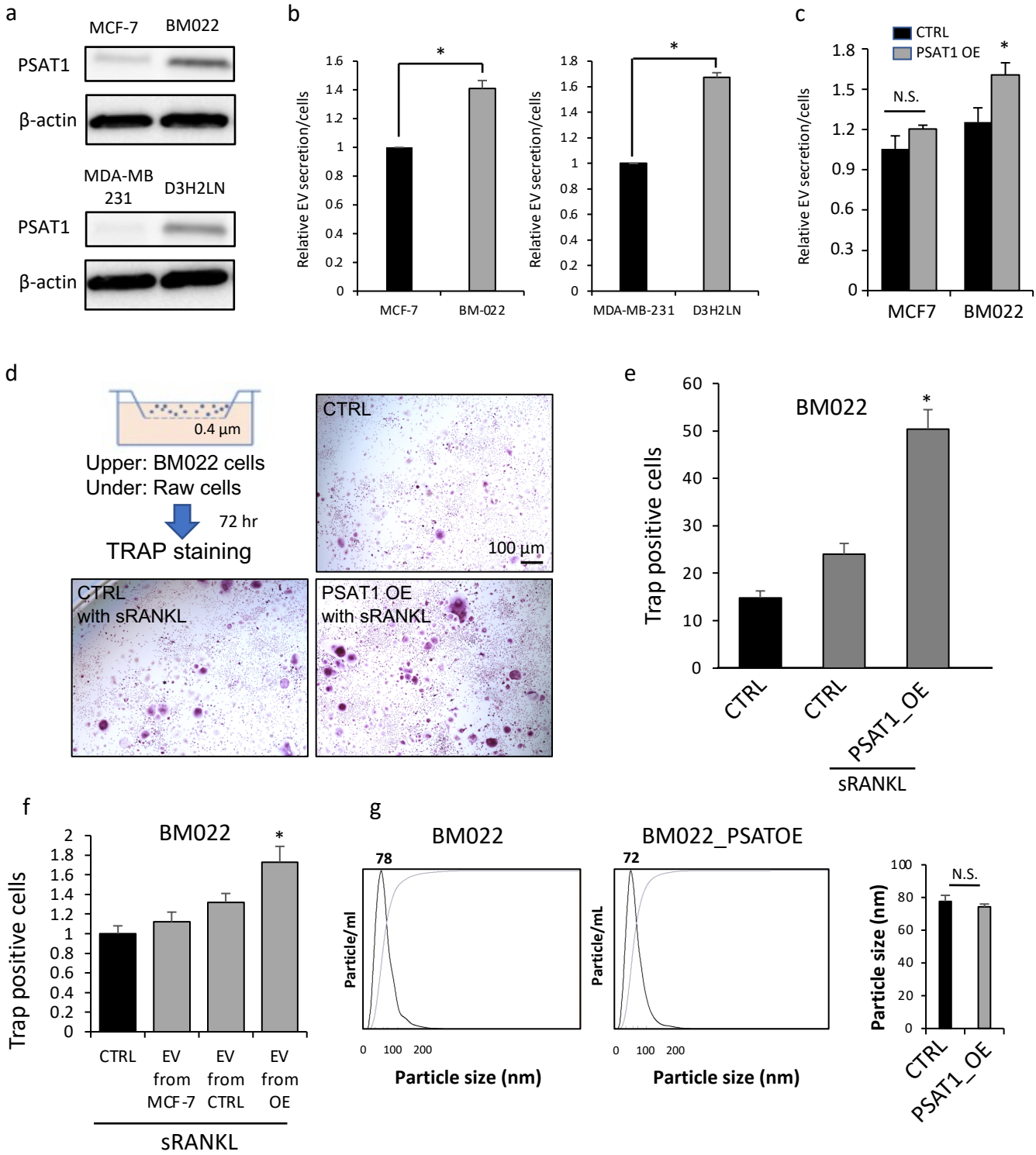
a
MCF-7
BM022
PSAT1
β-actin
MDA-MB 231
D3H2LN
PSAT1
β-actin
b
Relative EV secretion/cells
MCF-7
BM-022
MDA-MB-231
D3H2LN
c
CTRL
PSAT1 OE
N.S.
Relative EV secretion/cells
MCF7
BM022
d
0.4 µm
Upper: BM022 cells
Under: Raw cells
72 hr
TRAP staining
CTRL
100 µm
CTRL with sRANKL
PSAT1 OE with sRANKL
e
BM022
Trap positive cells
CTRL
CTRL
PSAT1_OE
sRANKL
f
BM022
Trap positive cells
CTRL
EV from MCF-7
EV from CTRL
EV from OE
sRANKL
g
BM022
78
Particle/ml
Particle size (nm)
BM022_PSATOE
72
Particle/mL
Particle size (nm)
N.S.
Particle size (nm)
CTRL
PSAT1_OE

Fig. 7

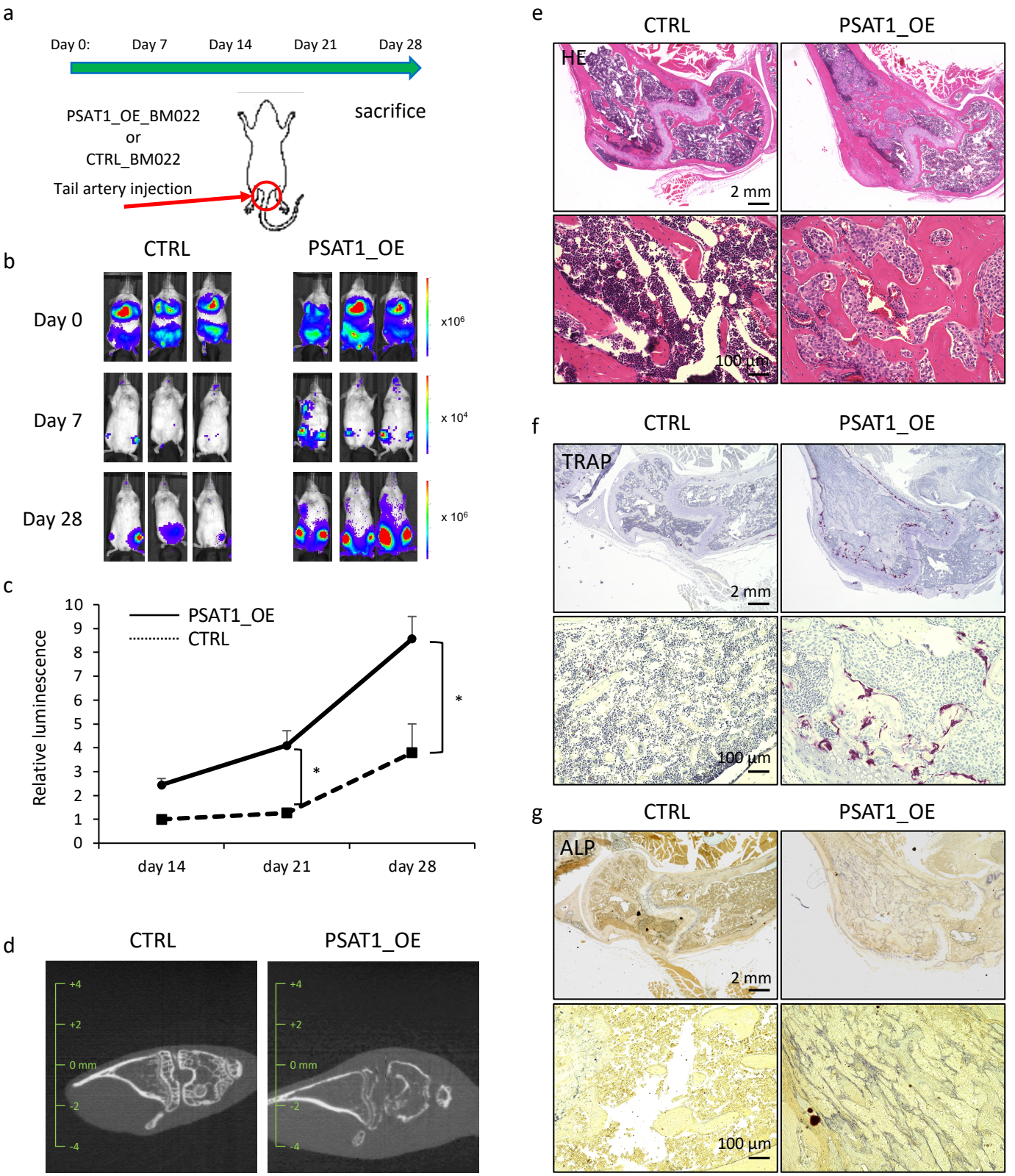
a
Day 0:
Day 7
Day 14
Day 21
Day 28
PSAT1_OE_BM022
or
CTRL_BM022
Tail artery injection
sacrifice
b
CTRL
PSAT1_OE
Day 0
Day 7
Day 28
x10⁶
x 10⁴
x 10⁶
c
PSAT1_OE
CTRL
Relative luminescence
0
1
2
3
4
5
6
7
8
9
10
*
*
day 14
day 21
day 28
d
CTRL
PSAT1_OE
+4
+2
0 mm
-2
-4
e
CTRL
PSAT1_OE
HE
2 mm
100 µm
f
CTRL
PSAT1_OE
TRAP
2 mm
100 µm
g
CTRL
PSAT1_OE
ALP
2 mm
100 µm